Chinese Journal of
POLYMER SCIENCE

RESEARCH ARTICLE

https://doi.org/10.1007/s10118-022-2880-4
Chinese J. Polym. Sci. **2023**, *41*, 962–971

Mechanically Robust Polylactide Fibers with Super Heat Resistance *via* Constructing *in situ* Nanofibrils

Jun Lu[a], Li-Xiang Yi[a], Yong-Huan Zhao[a], Yang Meng[a], Peng-Xiang Yu[a], Juan-Juan Su[a,b*], and Jian Han[a,b*]

[a] *College of Materials and Textiles, Zhejiang Sci-Tech University, Hangzhou 310018, China*
[b] *The Key Lab of Industrial Textile Material and Manufacturing Technology, Zhejiang Province, Zhejiang Sci-Tech University, Hangzhou 310018, China*

Electronic Supplementary Information

Abstract All-PLA fibers with excellent comprehensive performance and recycling convenience are realized efficiently. High molecular weight poly(D-lactide) (HPDLA) is incorporated into poly(L-lactide) (PLLA) matrix to construct *in situ* nanofibrils structure by taking advantages of the microphase separation between HPDLA and PLLA. The tensile strength of HPDLA/PLLA composite fibers (HDL-8) is enhanced from 2.1 cN/dtex of neat PLLA-8 fibers up to 2.9 cN/dtex. Its boiling water shrinkage (BWS) and shrinkage in hot air (HAS) significantly decrease to 7.8% and 2.8%, respectively. The abundance of *in situ* nanofibrils creates a grille-like structure that is crucial for both heat and hydrolysis resistance. More strikingly, a hybrid shish-kebab structure induced by the *in situ* nanofibrils serves as a mechanical reinforcement. This work paves a new way for heat resistance and self-reinforcement modification of PLA materials.

Keywords Polylactide fibers; Self-reinforcement; *In situ* nanofibrils; Heat resistance; Hybrid shish-kebab

Citation: Lu, J.; Yi, L. X.; Zhao, Y. H.; Meng, Y.; Yu, P. X.; Su, J. J.; Han, J. Mechanically robust polylactide fibers with super heat resistance *via* constructing *in situ* nanofibrils. *Chinese J. Polym. Sci.* **2023**, *41*, 962–971.

INTRODUCTION

It is imperative to vigorously develop biodegradable materials to address the issues caused by the energy crisis and environmental pollution. As a biodegradable and environmentally friendly polymer materials, poly(lactic acid) (PLA) has been a hot research topic for a while thanks to its excellent processibility, mechanical properties and good biocompatibility.[1–5] PLA is currently used in a variety of industries, including tissue engineering, textile and garment, packaging, agricultural mulch, 3D printing and so on.[6–10,15] It is challenging to control the crystallization of PLA due to their rigid main chains and weak crystallization ability, which makes it difficult to achieve high crystallinity under rapid cooling conditions. As a result, PLA products generally possess poor heat resistance, low mechanical properties, and are easily hydrolyzed.[3–6]

The most popular techniques for PLA modification include thermal annealing,[11–13] stereocomplex crystals (SCs),[4,14–16] nucleating agents,[5,17,18] and control of crystal morphology.[19–25] Even while annealing can improve the crystallinity, it has the drawbacks of being time-consuming and degrading mechanical properties caused on by disorientation.[13] The SCs, which are co-crystallized by poly(L-lactic acid) (PLLA) and poly(D-lactic acid) (PDLA), have a melting point (T_m) that is about 50 °C higher than homocrystals (HCs), and is widely used for heat resistance and reinforcing modification of PLA.[14–16] For instance, Li *et al*.[14] prepared PLA/poly(butylene adipate-*co*-terephthalate) (PBAT) blends with interfacial SCs through reactive blending, which enhanced mechanical properties and improved crystallization rates. To prepare PLA products with a high SCs content, however, is quite challenging due to the weak melt memory and low generation efficiency of SCs. Bai *et al*.[5] tailored crystal structure of PLLA fibers by using a nucleating agent of tetramethylene-dicarboxylic dibenzoyl-hydrazide (TMC-306). It could generate *in situ* nanofibrils to induce the crystallization of PLLA matrix and endow the PLLA fibers with good heat resistance and mechanical strength. However, the toughness of the modified PLLA fibers, which would be one of the crucial characteristics for the post-processing and application of PLLA fibers, was not reported. Also, the nucleating agents frequently used are organic small-molecule compounds with a certain degree of toxicity.

The *in situ* microfibrillar blends is a very effective method of polymer reinforcement modification, and its hierarchical structure control[25–31] is continue to stay the research hotspots. More recently, Yang *et al*.[25] prepared super-toughed PLA/thermoplastic poly(ester)urethane (TPU) blends by using an eccentric rotor extruder (ERE), which promoted the formation of *in situ* TPU nanofibrils. Li *et al*.[27] constructed PBAT *in*

* Corresponding authors, E-mail: sujuanjuan@zstu.edu.cn (J.J.S.)
E-mail: jianhan88@sina.cn (J.H.)

Received August 4, 2022; Accepted October 9, 2022; Published online December 12, 2022

situ nanofibrils in a PLA matrix by using the technique of "slit die extrusion-hot drawing-annealing drawing". The PLA/PBAT composites film exhibited good gas barrier performance and robust mechanical property. However, two incompatible polymers are commonly targeted in the *in situ* microfibrillar/nanofibrillar blends. Poor interfacial adhesion between the *in situ* microfibrils/nanofibrils and the matrix is caused by variations in chemical structure, surface tension, and viscoelasticity, which results in ineffective reinforcement.[29] Additionally, it raises the issues of prepared materials that cannot fully degrade or are not conducive to recycling, both of which are crucial factors to take into account for biodegradable materials.

Utilizing *in situ* microfibrillar technology for the fabrication of all-PLA blends would not only completely preserve degradability and prevent interfacial compatibility problems. The foundation for producing all-PLA composites with *in situ* microfibrils/nanofibrils is microphase separation. Chen *et al*.[32] discovered the microphase separation structure in the PLLA/PDLA blends. A stereoamorphous mesophase of PLA (sam-PLA) may be dispersed in the continuous PLLA or PDLA phases. The structure of the microphase separation of PLLA/PDLA blends is primarily influenced by stereoisomerism and molecular weight. As molecular weight increases, variations in melt viscoelasticity and molecular dynamics become more significant and are likely to result in a more pronounced phase separation. In order to construct *in situ* microfibrils/nanofibrils structures in all-PLA materials, we propose the introduction of high molecular weight PDLA (HPDLA) with many times the molecular weight of the matrix PLLA. To our knowledge, no studies have been reported on this issue. It is expected that this work would concurrently address the heat resistance and hydrolysis resistance issues as well as the self-reinforcement of PLA materials.

EXPERIMENTAL

Materials

All the materials used in this study are commercially available. Matrix PLLA, comprising 2% D-lactic acid (trade name 4032D), is purchased from Nature Works LLC. Its weight-average molecular weight (M_w) is 2.2×10^5 g/mol. HPDLA with a M_w of 5.5×10^5 g/mol is supplied by Jinan Daigang Biotechnology Co., LTD.

Sample Preparation

PLLA and HPDLA were respectively dissolved in dichloromethane, and then mixed with stirring until the solution was transparent. HPDLA/PLLA with a 1/4 weight ratio was fixed. Afterwards, the resulting solution was precipitated in excess ethanol to obtain white floc, which was then dried in a vacuum oven at 80 °C for 24 h. A two-stage melt spinning process was used to prepare fibers. Firstly, HPDLA/PLLA blends were extruded through the spinneret at 240 °C, and the fibers were collected with a take-up speed of 40 m/min around the godet. Secondly, the hot drawing process was carried out at 80 °C and the draw ratios (DR) were set as 4 and 8, while the take-up speed is kept consistent at 200 cm/min. For brevity, HPDLA/PLLA composite fibers with *X* times hot drawing were hereafter named as HDL-*X*. For example, the composite fibers after drawn for 4 times was called as HDL-4. Meanwhile, the control sample of neat PLLA fibers were also prepared according to the same method as above mentioned. The fineness of PLLA and HDL fibers are shown in Table S1 (in the electronic supplementary information, ESI).

Characterization

The morphology was characterized by scanning electron microscope (FE-SEM, VeriosG4) at the voltage of 3.0 kV and samples were sputter-coated with a thin gold layer to imaging. The melt filaments extruded through spinneret were cryo-fractured by immersing in liquid nitrogen for 1 h. To observe crystalline morphology in HDL fibers, they were etched by a water/methanol (1/1, *V*/*V*) solution containing 0.05 mol/L of sodium hydroxide for 24 h at room temperature.

The crystal structures were investigated by two-dimensional wide angle X-ray diffraction (2D-WAXD) using a Bruker D8 Discover X-ray diffractometer equipped with a Vantec 500 detector. The crystal orientation was quantified on the basis of Herman's orientation parameter (f_H) using the following equations:

$$f_H = \frac{3\left(\cos^2\varphi\right) - 1}{2} \tag{1}$$

$\cos^2\varphi$ is an orientation factor defined as

$$\cos^2\varphi = \frac{\int_0^{\frac{\pi}{2}} I(\varphi)\sin\varphi\cos^2\varphi \mathrm{d}\varphi}{\int_0^{\frac{\pi}{2}} I(\varphi)\sin\varphi \mathrm{d}\varphi} \tag{2}$$

where φ is the azimuthal angle and $I(\varphi)$ is the scattering intensity along the angle φ.

The sound velocity orientation is tested by SCY-III. The time of sound velocity propagation at 20 and 40 cm of each fiber was measured, respectively. Orientation factor of sound velocity was calculated by the following equation:

$$f_s = 1 - \frac{{C_u}^2}{C^2} \tag{3}$$

where the sound velocity C_u for random orientation was taken as 1.3 km/s of PLLA-0 sample.

The non-isothermal crystallization behaviors were conducted on a DSC-8000 Instrument (Perkin Elmer) under dry nitrogen atmosphere. Samples with a weight of about 5 mg were heated from 25 °C to 260 °C with a heating rate of 10 °C/min. The crystallinity of HC-PLA (X_{hc}) and SC-PLA (X_{sc}) was calculated as:

$$X_{hc}(\%) = \frac{\Delta H_{hc} - \Delta H_{cc}}{\Delta H^0_{m,hc}} \times 100\% \tag{4}$$

$$X_{sc}(\%) = \frac{\Delta H_{sc}}{\Delta H^0_{m,sc}} \times 100\% \tag{5}$$

where ΔH_{hc} and ΔH_{sc} are the melting enthalpies of the HC-PLA and SC-PLA crystallite, ΔH^0_m is the theoretical value of melting enthalpy for 100% crystalline HC-PLA and SC-PLA. The values are used as 93.7 and 142 J/g, respectively. The total crystallinity (X_c) is evaluated as:

$$X_c(\%) = X_{hc} + X_{sc} \tag{6}$$

The crystal morphology of pure PLLA-8 and HDL-8 fibers after hot pressing at 200 °C was observed by Leica DMLP polarizing microscope.

Tensile mechanical properties were tested at room temper-

ature using an Instron-3369 universal testing machine (U.K.) with a crosshead speed of 50 mm/min and a gauge length of 20 mm. For each fiber, 10 samples were performed and the average results was reported.

Thermal shrinkage tests were performed by boiling water shrinkage (BWS) and shrinkage in hot air (100 °C) (HAS). During the testing of BSW, fibers were immersed in boiling water for 30 min without any tension and then kept at room temperature for 20 min. The shrinkage in hot air was measured by heating the fibers in an oven with a temperature of 100 °C for 30 min without any tension. The shrinkage was obtained by the following equation:

$$\text{Shrinkage (\%)} = \frac{(L_0 - L)}{L_0} \times 100\% \quad (7)$$

where L_0 is the original length, L is the final length.

To study the hydrolysis resistance, the HDL-8 and PLLA-8 fibers were treated in aqueous solution with pH 12 at 70 °C for 24, 48, 72 and 96 h, respectively. Then, each sample was washed with distilled water and dried at ambient temperature. The mass loss rate after hydrolysis was calculated according to the following relationship:

$$\Delta W = \frac{(m_0 - m)}{m_0} \times 100\% \quad (8)$$

where m_0 is the quality of fibers before hydrolysis; m is the quality of fibers after hydrolysis.

RESULTS AND DISCUSSION

In situ Nanofibrils Structure

SEM observation was carried out on melt blends of HPDLA and PLLA to explore the microphase separation structure, which is the basis for the construction of *in situ* microfibrils or nanofibrils structures. As shown in Fig. S1 (in ESI), a typical sea-island morphology can be observed in the cryofracture surface of HPDLA/PLLA melting filament. It indicates that HPDLA with high molecular weight and viscoelasticity can be phase separated in the PLLA matrix, and the dispersed phase size is about 2 μm. Our work is the first to discover the microphase separation of HPDLA and PLLA during melt processing. In our opinion, the dispersed phase should consist mainly HPDLA with a small amount of PLLA. Phase separation mechanism research and more thorough microstructure characterization are currently being followed up. Fig. 1 depicts the morphology of HDL

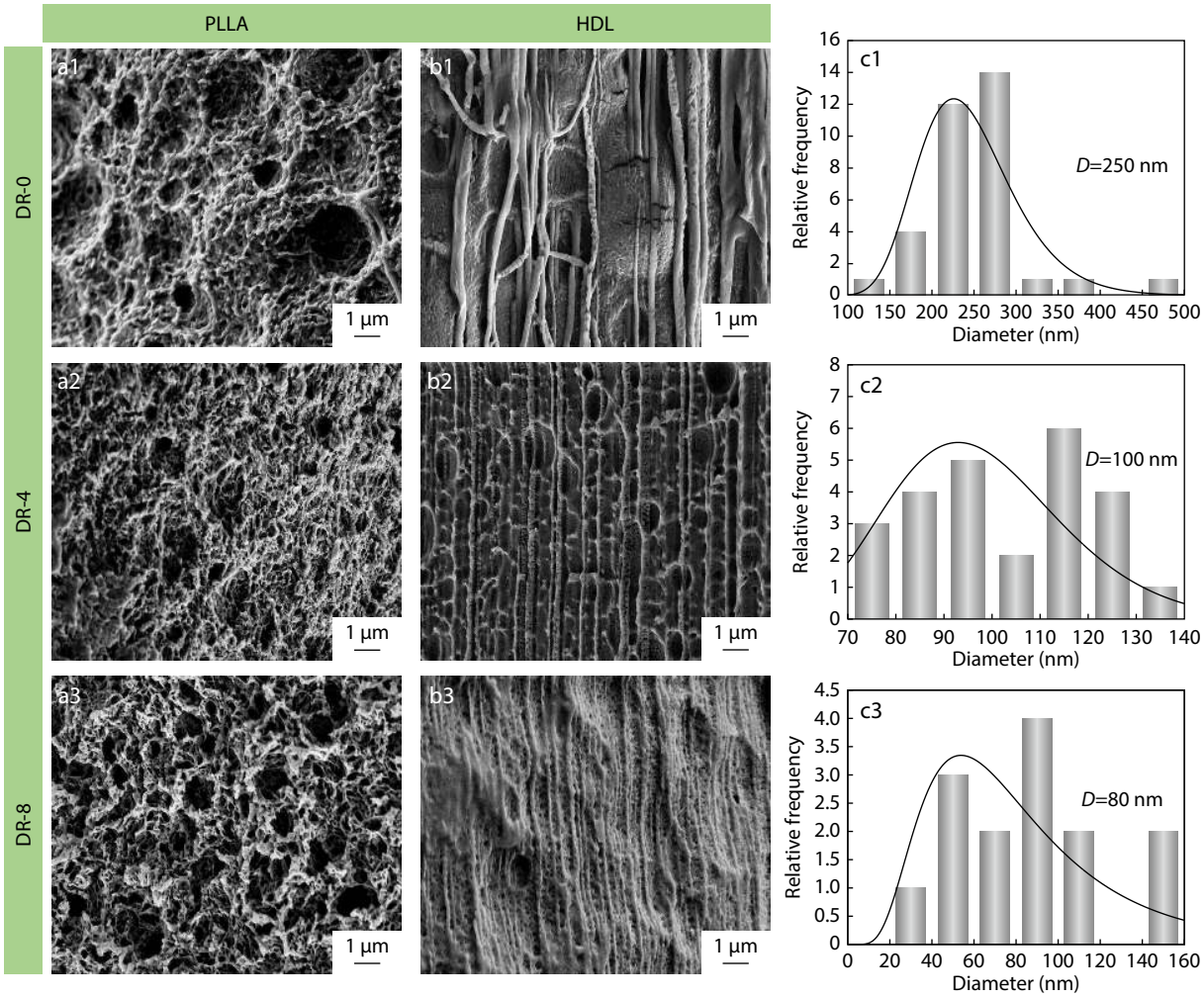

Fig. 1 SEM images of fibers with different DRs etched by sodium hydroxide: (a) neat PLLA fibers, (b) HDL composite fibers; (c) Diameter distribution of nanofibrils.

https://doi.org/10.1007/s10118-022-2880-4

composite fibers with various DRs after etching. In contrast to the irregular porous structure in the pure PLLA fibers, *in situ* microfibrils with an average diameter of 250 nm are detected in the HDL composite fibers. In general, if the viscosity of the dispersed phase is much higher than that of the matrix phase, extensional stress is not conducive to act on the dispersed phase and drag it to deform into microfibrils. In this work, however, there may be more molecular chain entanglements at the interface between the continuous and dispersed phases. Which greatly improves the interfacial stress transfer and makes the stress work more effectively on the dispersed phases with high-viscosity, thus dragging the spherical dispersed phases into *in situ* microfibrils. It can be deduced from the morphology observation of Figs. 1(b2) and 1(b3) that the hot drawing-induced extensional stress causes the microfibrils to further deform into nanofibrils. The diameter of *in situ* nanofibrils decreases from the initial 250 nm of HDL-0 to 100 nm of HDL-4 as well as even 80 nm of HDL-8 fibers. The *in situ* nanofibrils also arrange more closely and orderly may owing to that the hot drawing temperature (80 °C) is higher than the glass transition temperature (T_g: 60–65 °C) of PLLA and HPDLA. Up to this point, a grille-like structure, assembled by rich and orderly *in situ* nanofibrils, has been constructed in the HDL-8 composite fibers under the extensional stress field of melt spinning and subsequent hot drawing.

Orientation Structure

WAXD is utilized to detect the oriented crystalline structure. Fig. 2 exhibits the 2D-WAXD patterns of the PLLA and HDL fibers before and after hot-drawing. 1D-WAXD curves are integrated circularly from the corresponding 2D-WAXD patterns as shown in Fig. S2 (in ESI). Only amorphous halo diffraction exists in as-spun PLLA and HDL fibers, suggesting the very low crystallinity under the weak extensional stress of melt spinning process. Two characteristic diffraction peaks (2θ about 17° and 19°) of HCs present in both PLLA and HDL fibers with DRs of 4 and 8. Additionally, the diffraction peak (2θ around 24°) of SCs exits in HDL-4 and HDL-8 fibers, yet it is not easily visualized even with DR increasing. It suggests that strong extensional stress of hot drawing could predominantly evoke crystallization of HCs.[33] With the increasing DR, the symmetric diffraction spots around the meridian appear and get stronger on both neat PLLA and HDL composite fibers, manifesting the formation of oriented crystals. The Herman's orientation parameter (f_H) of (200/110) reflection assigned to HCs is calculated as shown in Fig. 3(a). The f_H of PLLA and HDL fibers improves with increasing DR. The crystal orientation of HDL fibers is somewhat higher than that of PLLA fibers when the DR is 4, while the f_H of the HDL-8 composite fibers is nearly identical to PLLA-8 fibers. This indicates that *in situ* nanofibrils may not make contribution on the crystal orientation of the HDL composite fibers. Certainly, under the strong extensional stress by hot-drawing, strain-induced orientation and crystallization of HCs is visibly took place. Which generates abundant oriented HCs crystallites verified by an increasing f_H.

The orientation of the molecular chains is one of the important structural parameters governing the performance of polymer fibers. The sound velocity method was utilized to further characterize the orientation of molecular chains averaged in the crystalline and amorphous phases. As presented in Fig. 3(b), the sound speed orientation factor (f_S) of both PLLA and HDL fibers improves with increasing DR. The f_S of HDL composite fibers, however, is significantly higher than that of pure PLLA fibers with equal DR. Especially when DR is 8, the f_S of the HDL fibers is up to 77.2%, in contrast to 37.6% for the PLLA fibers. When DR is 4 or 8, it is presumed that HDL fibers have a stronger molecular orientation in the amorphous phases than that of PLLA fibers, after all, they have comparable crystalline orientation shown as WAXD results. In our view, the improved amorphous molecular orientation of the HDL composite fibers could be attributed to the following. First, HPDLA molecules, mainly available in *in situ* microfibrils and nanofibrils, have a longer relaxation time due to its higher molecular weight. Second, grille-like structure with abundant nanofibrils could constrain the movement of PLLA mo-

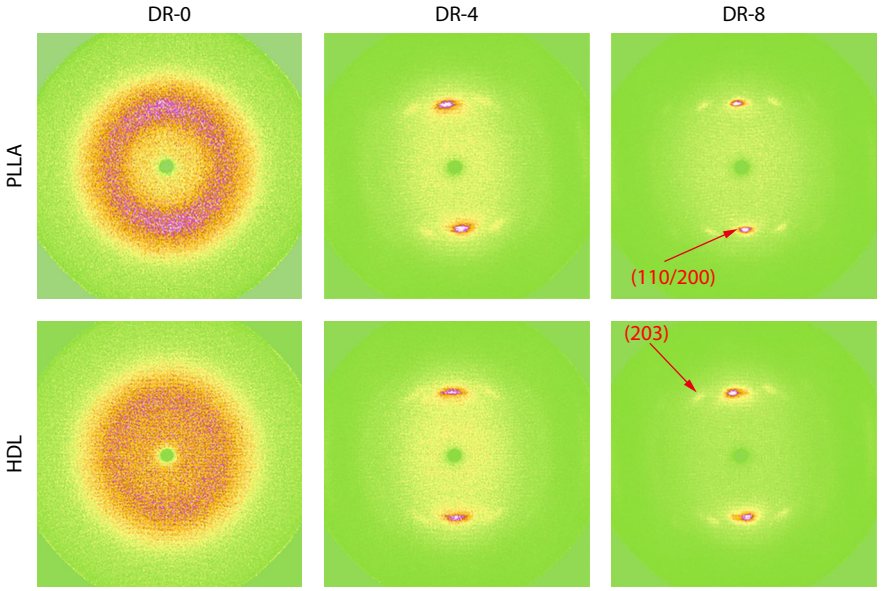

Fig. 2 2D-WAXD patterns of fibers with various DRs. The fiber axis is horizontal.

https://doi.org/10.1007/s10118-022-2880-4

lecules between the nanofibrils space. These finally result in readily maintaining of molecular orientation in the amorphous phases of HDL fibers under extensional stress.

Crystallization Behavior

Fig. 4 and Table S2 (in ESI) show the DSC curves and data summary of prepared PLA fibers. In the DSC curves of HDL composite fibers (Fig. 4b), an obvious endothermic peak is discovered around T_g, and the endothermic enthalpy of the as-spun fiber is the most evident. As far as we are concerned, this endothermic peak could be primarily attributed to the relaxation of oriented HPDLA chains, which are severely confined within *in situ* microfibrils and nanofibrils.[33] The cold crystallization temperature (T_{cc}) of HDL-0 composite fibers is lower by about 12 °C compared with that of PLLA-0 fibers. The SCs in the composite fibers can act as nucleating agents to induce the HCs crystallization of PLLA and HPDLA. The T_{cc} peaks of the HDL composite fibers are absent, at DR 4 or 8, while obvious ones exist for neat PLLA fibers. The crystallinity of HDL-4 composite fibers is up to 40% and about 10% higher than that of neat PLLA-4 fibers. This demonstrates more obvious strain-

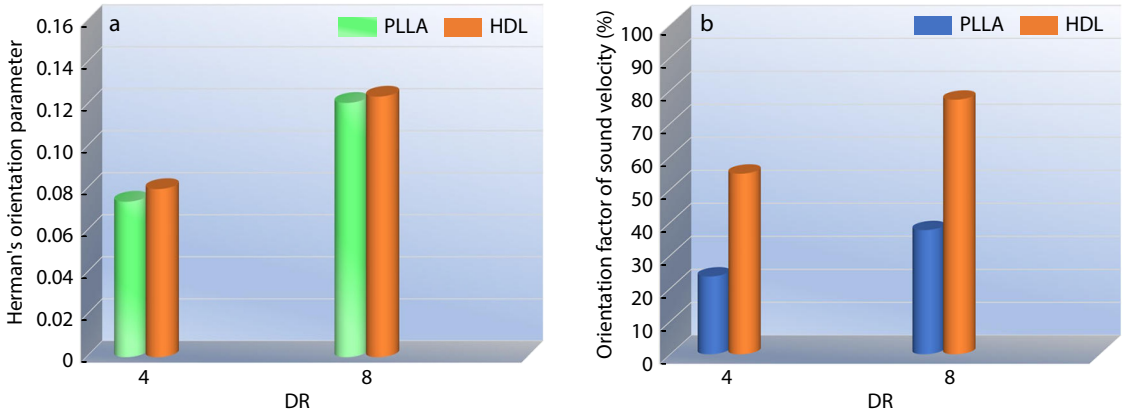

Fig. 3 (a) Herman's orientation parameter obtained from 2D-WAXD; (b) Sound velocity orientation of fibers with various DRs.

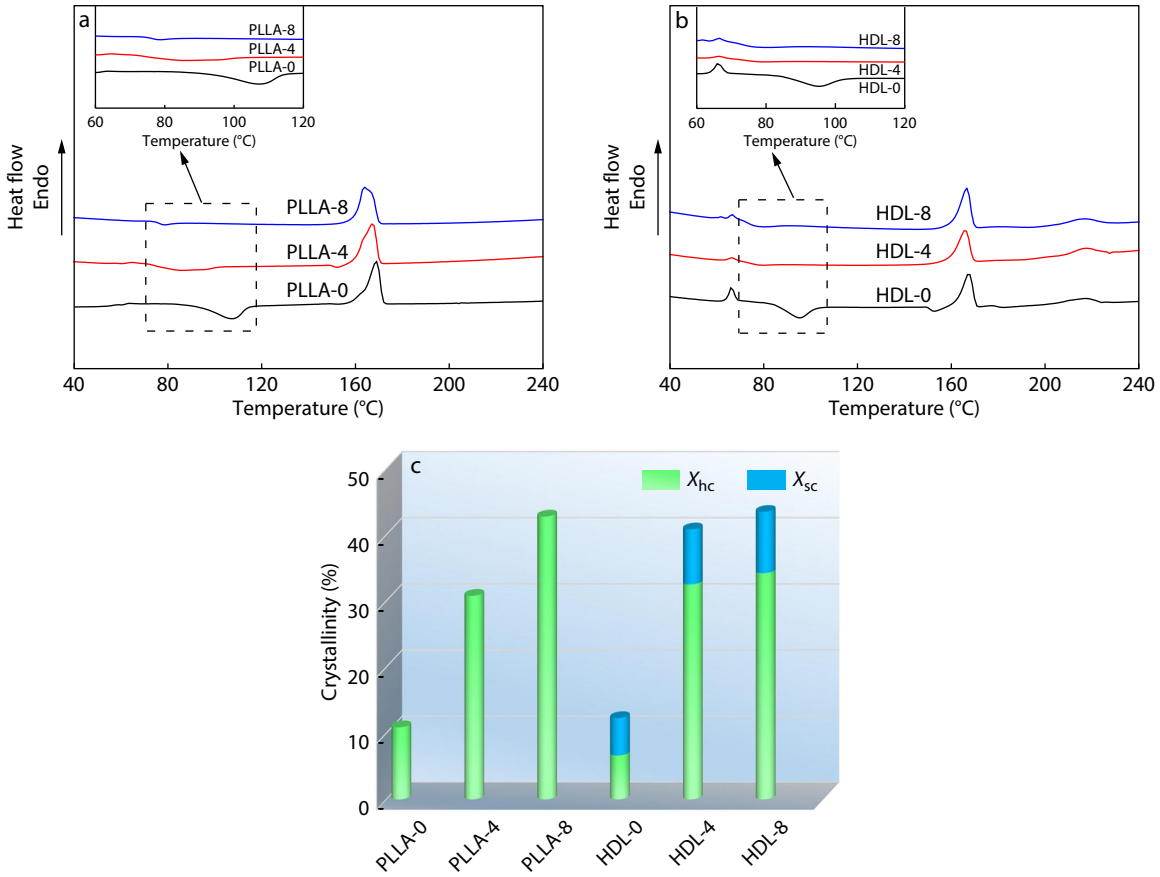

Fig. 4 DSC curves of (a) neat PLLA fibers and (b) HDL composite fibers with various DRs; (c) The crystallinity results calculated from corresponding curves.

https://doi.org/10.1007/s10118-022-2880-4

induced orientation and crystallization in HDL fibers with assistance of *in situ* fibrils.[33–35] The SCs crystallinity of the composite fibers is relatively low within the range of 5%–10%. In our work, the content ratio of HPDLA to PLLA (1:4), which is far from the optimal ratio (1:1), as well as the much higher molecular weight of HPDLA are not favorable for SCs crystallization.[36] The SCs crystallinity increases from 5.57% of HDL-0 fiber to 9.35% of HDL-8 fiber. With increasing DR, the increased specific surface area of the *in situ* nanofibrils improves the contact probability between HPDLA and PLLA molecules on the one hand, and on the other hand, the strong molecular orientation facilitates the SCs crystallization. To further investigate the morphology of SCs, HDL-8 composite fibers and neat PLLA-8 fibers were heat treated at 200 °C ($T_{m,hc}<T<T_{m,sc}$), under which HCs were melted while SCs could sustain. As shown in Fig. 5, abundant SCs exist in HDL-8 fibers, while they cannot be exactly located due to the limited magnification of the POM. However, it is preferred that SCs mainly distribute inside the nanofibrils and on the interface along the fiber axis.

Mechanical Behavior and Reinforcing Mechanism

As shown in Fig. 6, the tensile strength of the HDL fibers is significantly higher than that of pure PLLA fibers. The tensile strength of HDL-8 fibers improves from 2.1 cN/dtex of PLLA-8 fibers to 2.9 cN/dtex, while its elongation at break stays high at 100%, displaying an exceptional balance of strength and toughness. The microstructure of the fibers after tensile fracture is investigated more thoroughly in order to further interpret the mechanical performance. Fig. 7 clearly reveals that the crystallinity of the HDL composite fibers is remarkably increased after stretched. Even for highly crystallized HDL-8 sample, the crystallinity enhances from 43% to 52% after stretched with a noticeable strain-induced crystallization. The crystalline structure induced by tensile stretching was confirmed by SEM. The nanofibrils in the HDL composite fibers are further refined with reduced diameter at the tensile stress (Fig. 7d). More strikingly, abundant denser hybrid shish-kebab crystallites arranged as interlocking network structures are observed in both HDL-4 and HDL-8 fibers. This indicates that highly oriented nanofibril serves as shish to induce the crystallization of matrix PLLA molecules as kebab. As shown in Figs. 7(d2) and 7(d3), the diameter of the nanofibril-shish is much finer and the kebab is also thicker in HDL-8 fibers than that in HDL-4 fibers. Additionally, the interlocking network structure assembled by hybrid shish-kebab is regular and compact most in HDL-8 fibers.

The mechanism diagram in Fig. 8 is used to illustrate the deformation process of nanofibrils structure and the generation mechanism of hybrid shish-kebab. The melt blends of HPDLA/PLLA undergo visible phase separation due to the considerably higher molecular weight of HPDLA than PLLA and their different optical isomerism. During the melt spinning process, the HPDLA/PLLA melting filament is subjected to an external stress, allowing the spherical and highly viscous dispersed phases to be dragged and deformed into *in situ* microfibrils. During hot drawing with stronger extensional stress, the *in situ* microfibrils further deform into nanofibrils. In the tensile stress, the further refined nanofibril acts as shish to induce the surrounding highly oriented molecules to crystallize on its surface to generate a hybrid shish-kebab structure. The abundant nanofibrils-shish results in an interlocking network structure of the hybrid shish-kebab, which serves as an excellent self-reinforcement to the all-PLA fibers.

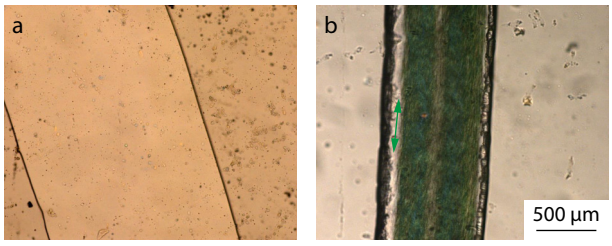

Fig. 5 POM micrographs of neat PLLA-8 fibers (a) and HDL-8 fibers (b) after treated at 200 °C.

Heat Resistance and Hydrolysis Resistance

As presented in Fig. 9, a very prominent reduction in both BWS and HAS of HDL composite fibers compared to PLLA fibers is observed. Specifically, the BWS and HAS of HDL-8 fibers are reduced to 7.8% and 2.8%, compared to 20.8% and 15.6% of PLLA-8 fibers, respectively. The improved heat resistance of PLA fibers is highly essential for either post processing or application. Taking the fibers with DR 8 as examples, the mechanism for the above-mentioned heat resistance improvement is analyzed. Taking into account the comparable crystallinity and crystalline orientation of the HDL-8 and PLLA-8 fibers, it implies that these two structure factors should not be

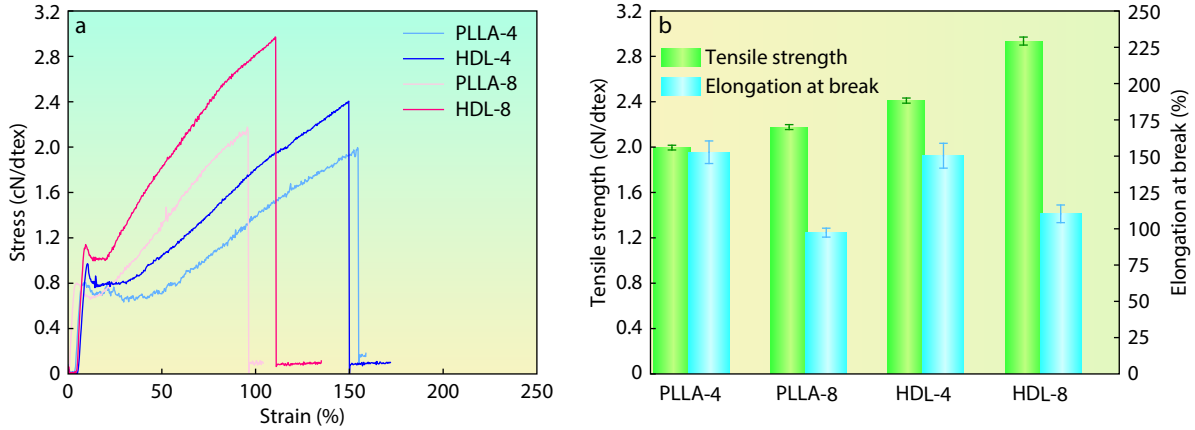

Fig. 6 (a) Stress-strain curves and (b) tensile properties of neat PLLA and HDL composite fibers.

https://doi.org/10.1007/s10118-022-2880-4

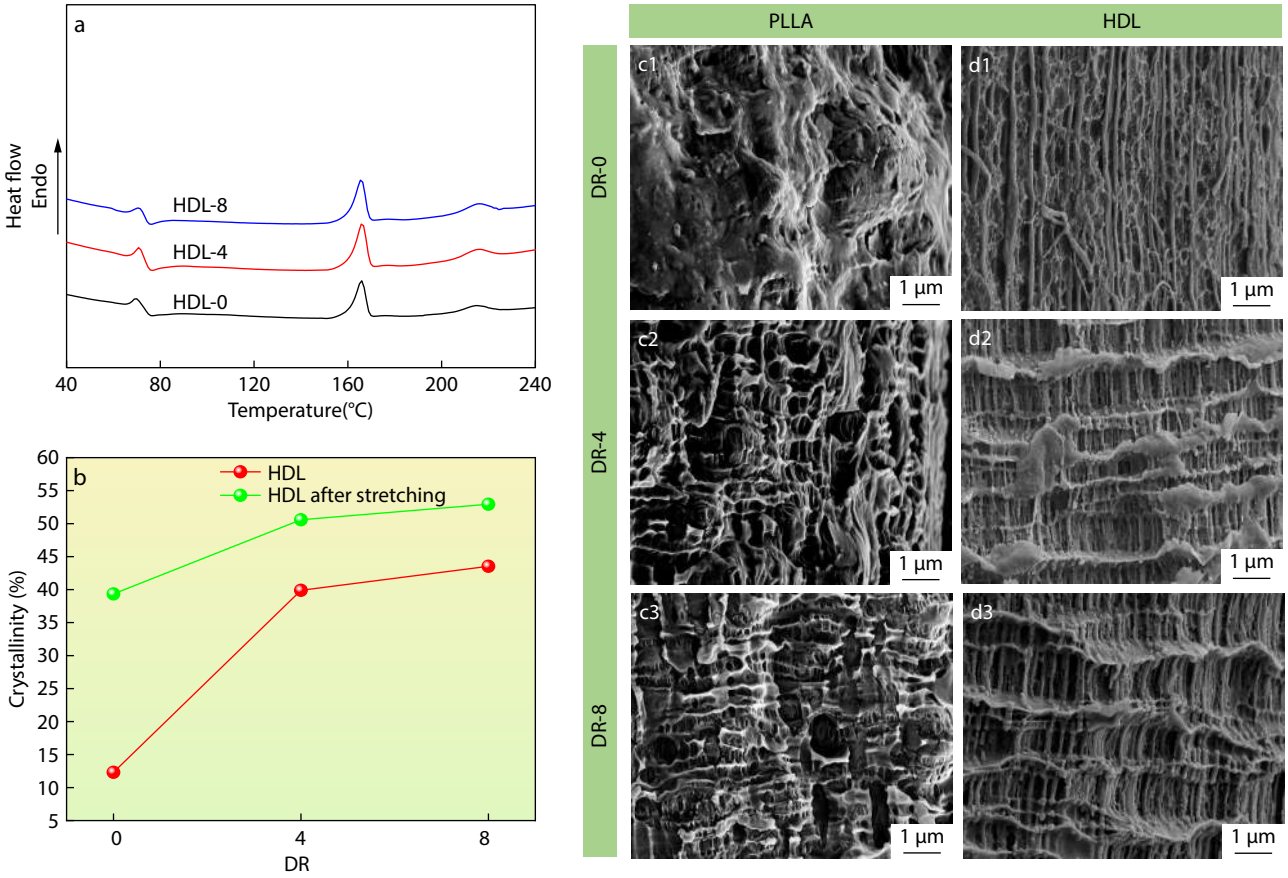

Fig. 7 (a) DSC curves and (b) crystallinity of HDL composite fibers after tensile tested; SEM images of fibers after tensile tested: (c) neat PLLA, (d) HDL composite fibers.

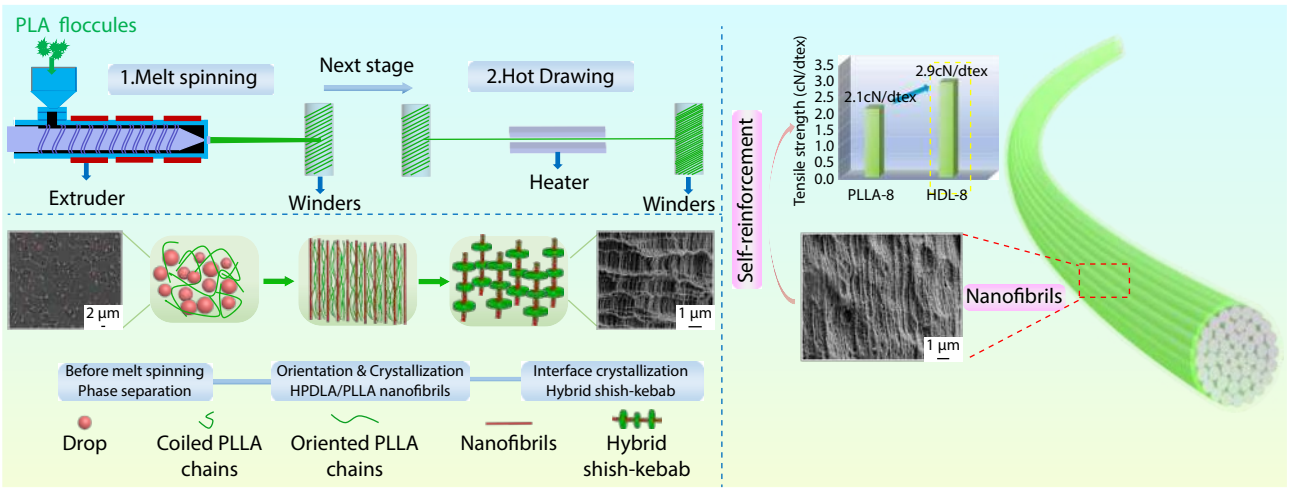

Fig. 8 Schematic diagram for the deformation of nanofibrils structure and the generation mechanism of hybrid shish-kebab.

considered as the main contributors to heat resistance improvement of the HDL fibers. The thermal shrinkage of polymer fibers, essentially, is driven by high elastic recoiling of oriented amorphous molecular chains. This is very appropriate to realize the improved heat resistance by restricting the moving of molecular segments. In our work, the closely arranged grille-like structure can greatly confine the moving and recoiling of oriented amorphous PLLA molecules. The HPDLA molecular chains within the nanofibrils, simultaneously, are limited to recoiling by reason of the restricted nanometer size of *in situ* nanofibrils. In contrast, neat PLLA fibers, which is not well structured for restricting the recoiling of oriented amorphous molecules, exhibit much higher thermal shrinkage.

Hydrolysis resistance of PLA is of great importance since that water molecules could attack the ester groups to breaking into carboxyl and hydroxyl groups. The hydrolyzed carboxyl groups could further catalyze the hydrolysis process in particular heat and alkaline conditions. The mass loss (ΔW)

https://doi.org/10.1007/s10118-022-2880-4

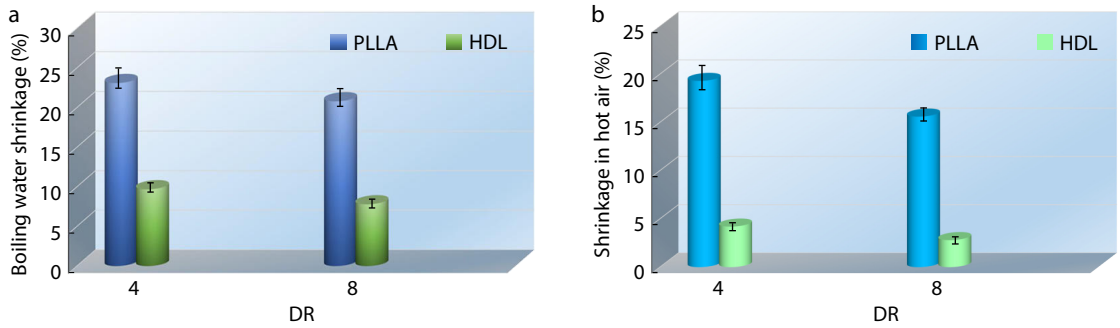

Fig. 9 (a) Boiling water shrinkage and (b) shrinkage in hot air of fibers with various DRs.

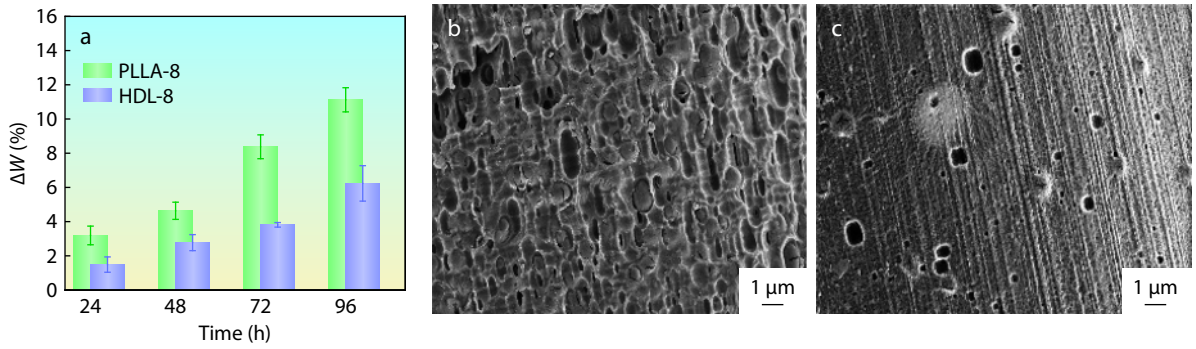

Fig. 10 (a) The mass loss rate (Δ*W*) of fibers (DR-8) after hydrolysis in aqueous solution. SEM images of fibers (DR-8) after hydrolysis 96 h: (b) neat PLLA fibers, (c) HDL composite fibers.

of PLLA-8 and HDL-8 fibers after hydrolysis in aqueous solution is shown in Fig. 10(a). The ΔW of HDL-8 fibers, within the observation time, is evidently lower compared to PLLA-8 fibers. After hydrolysis for 96 h, the ΔW of HDL-8 fibers is super-low as 6.24%, while it is quite-high as 11.12% for PLLA-8 fibers. The hydrolysis resistance of the HDL-8 composite fibers is substantially improved. In order to further explore the hydrolysis mechanism, the surface morphology and microstructure of the hydrolyzed fibers are conducted. The surface morphology of hydrolyzed PLLA-8 and HDL-8 fibers is shown in Fig. 10. After hydrolysis, the surface of PLLA-8 fibers is covered with submicron pits. In striking contrast, a small number of pits are sporadically distributed on the surface of HDL-8 fibers. As shown in Fig. S3 (in ESI), the crystallinity of both PLLA-8 and HDL-8 fibers increases very markedly after hydrolysis. This is reasonable given that the molecules of the amorphous region are more likely to be attacked by water molecules and then hydrolyzed. The HPDLA is less susceptible to hydrolysis as the higher the molecular weight, the better the resistance to hydrolysis. The nanofibrils grille-like structure plays a certain barrier effect on the invasion of water molecules, which effectively improves the hydrolysis resistance of HDL composite fibers.

CONCLUSIONS

This work demonstrates a novel way to construct the *in situ* nanofibrils to realize the self-reinforcement and heat resistance improvement of all-PLA fibers. There is a visible phase separation in HPDLA/PLLA melt blends, and the spherical dispersed phases could be deformed into *in situ* nanofibrils during melt spinning and subsequent hot drawing. An interlocking network structure of the hybrid shish-kebab induced by nanofibrils under tensile stress is discovered. Which has an outstanding strengthening effect on HDL-8 composite fibers, with a 38% increase in tensile strength compared to pure PLLA-8 fibers. Furthermore, the abundant nanofibrils assemble as a grille-like structure, which can greatly improve the heat resistance of the composite fibers by restricting the recoiling of oriented amorphous molecules. The BWS and HAS of HDL-8 fibers are low to 7.7% and 2.8%, respectively. The grille-like structure simultaneously acts as a physical barrier to water molecules, making the composite fibers significantly more resistant to hydrolysis. In conclusion, this work has produced mechanically robust all-PLA fibers also with super heat and hydrolysis resistance. This not only facilitates the industrial application of PLA fibers, but also opens up ideas for the recycling of waste PLA fibers.

NOTES

The authors declare no competing financial interest.

Electronic Supplementary Information

Electronic supplementary information (ESI) is available free of charge in the online version of this article at http://doi.org/10.1007/s10118-022-2880-4.

ACKNOWLEDGMENTS

This work was financially supported by the Natural Science

Foundation of Zhejiang Province (No. LGG21E030013) and Postdoctoral Research Foundation of China (No. 2019-M662111).

REFERENCES

1 Yang, Z. T.; Yang, J. X.; Fan, J. H.; Feng, Y. H.; Huang, Z. X. Preparation of super-toughened poly(L-lactide) composites under elongational flow: a strategy for balancing stiffness and ductility. *Compos. Sci. Technol.* **2021**, *208*, 108758.
2 Zhou, L.; Xu, P. P.; Ni, S. H.; Xu, L.; Lin, H.; Zhong, G. J.; Huang, H. D.; Li, Z. M. Superior ductile and high-barrier poly(lactic acid) films by constructing oriented nanocrystals as efficient reinforcement of chain entanglement network and promising barrier wall. *Chinese J. Polym. Sci.* **2022**, *40*, 1201–1212.
3 Bai, H. W.; Huang, C. M.; Xiu, H.; Gao, Y.; Zhang, Q.; Fu, Q. Toughening of poly(l-lactide) with poly(ε-caprolactone): combined effects of matrix crystallization and impact modifier particle size. *Polymer* **2013**, *54*, 5257–5266.
4 Zhang, H. X.; Bai, H. W.; Deng, S. H.; Liu, Z. W.; Zhang, Q.; Fu, Q. Achieving all-polylactide fibers with significantly enhanced heat resistance and tensile strength *via in situ* formation of nanofibrilized stereocomplex polylactide. *Polymer* **2019**, *166*, 13–20.
5 Zhang, H. X.; Bai, H. W.; Liu, Z. W.; Zhang, Q.; Fu, Q. Z.; Liu, Q.; Zhang, X.; Fu. Q. Toward high-performance poly(L-lactide) fibers *via* tailoring crystallization with the aid of fibrillar nucleating agent. *ACS Sustain. Chem. Eng.* **2016**, *4*, 3939–3947.
6 Xue, B.; He, H. Z.; Huang, Z. X.; Zhu, Z. W.; Xue, F.; Liu, S. M.; Liu, B. D. Fabrication of super-tough ternary blends by melt compounding of poly(lactic acid) with poly(butylene succinate) and ethylene-methyl acrylate-glycidyl methacrylate. *Compos. B Eng.* **2019**, *172*, 743–749.
7 Yang, J.; Li, W.; Mu, B. N.; Xu, H. L.; Hou, X. L.; Yang, Y. Q. 3D printing of toughened enantiomeric PLA/PBAT/PMMA quaternary system with complete stereo-complexation: compatibilizer architecture effects. *Polymer* **2022**, *242*, 124590.
8 Khosravi, A.; Fereidoon, A.; Khorasani, M. M.; Naderi, G.; Ganjali, M. R.; Zarrintaj, P.; Saeb, M. R.; Gutiérrez, T. J. Soft and hard sections from cellulose-reinforced poly(lactic acid)-based food packaging films: a critical review. *Food Packag. Shelf Life* **2020**, *23*, 100429.
9 Vlierberghe, S. V.; Dubruel, P.; Schacht, E. Biopolymer-based hydrogels as scaffolds for tissue engineering applications: a review. *Biomacromolecules* **2011**, *12*, 1387–1408.
10 Kurokawa, N.; Hotta, A. Thermomechanical properties of highly transparent self-reinforced polylactide composites with electrospun stereocomplex polylactide nanofibers. *Polymer* **2018**, *153*, 214–222.
11 Furuhashi, Y.; Kimura, Y.; Yoshie, N.; Yamane, H. Higher-order structures and mechanical properties of stereocomplex-type poly(lactic acid) melt spun fibers. *Polymer* **2006**, *47*, 5965–5972.
12 Zakir Hossain, K. M.; Parsons, A. J.; Rudd, C.D.; Ahmed, I.; Thielemans, W. Mechanical, crystallisation and moisture absorption properties of melt drawn polylactic acid fibres. *Eur. Polym. J.* **2014**, *53*, 270–281.
13 Na, B.; Tian, N. N.; Lv, R. H.; Zou, S. F.; Xu, W. F.; Fu, Q. Annealing-induced oriented crystallization and its influence on the mechanical responses in the melt-spun monofilament of poly(l-lactide). *Macromolecules* **2010**, *43*, 1156–1158.
14 Chen, J. L.; Rong, C. Y.; Lin, T. T.; Chen, Y. H.; Wu, J. L.; You, J. C.; Wang, H. T.; Li, Y. J. Stable co-continuous PLA/PBAT blends compatibilized by interfacial stereocomplex crystallites: toward full biodegradable polymer blends with simultaneously enhanced mechanical properties and crystallization rates. *Macromolecules* **2021**, *54*, 2852–2861.
15 Li, J. F.; Ye, W. Y.; Fan, Z. Y.; Cao, L. A novel stereocomplex poly(lactic acid) with shish-kebab crystals and bionic surface structures as bioimplant materials for tissue engineering applications. *ACS Appl. Mater. Interfaces* **2021**, *13*, 5469–5477.
16 Deng, S. H.; Yao, J.; Bai, H. W.; Xiu, H.; Zhang, X.; Fu, Q. A generalizable strategy toward highly tough and heat-resistant stereocomplex-type polylactide/elastomer blends with substantially enhanced melt processability. *Polymer* **2021**, *224*, 123736.
17 Chen, Y.; Hua, W. Q.; Zhang, Z. C.; Xu, J. Z.; Bian, F. G.; Zhong, G. J.; Xu, L.; Li, Z. M. An efficient, food contact accelerator for stereocomplexation of high-molecular-weight poly(L-lactide)/poly(D-lactide) blend under nonisothermal crystallization. *Polymer* **2019**, *170*, 54–64.
18 He, D. G.; Wang, Y. M.; Shao, C. G.; Zheng, G. Q.; Li, Q.; Shen, C. Y. Effect of phthalimide as an efficient nucleating agent on the crystallization kinetics of poly(lactic acid). *Polym. Test.* **2013**, *32*, 1088–1093.
19 Kuang, T. R.; Zhang, M. L.; Lian, X. H.; Zhang, J. B.; Liu, T.; Zhang, S. D.; Peng, X. F. External flow-induced highly oriented and dense nanohybrid shish-kebabs: a strategy for achieving high performance in poly(lactic acid) composites. *Compos. Commun.* **2022**, *29*, 101042.
20 Shahnooshi, M.; Javadi, A.; Nazockdast, H.; Ottermann, K.; Altstadt, V. Rheological rationalization of *in-situ* nanofibrillar structure development: tailoring of nanohybrid shish-kebab superstructures of poly(lactic acid) crystalline phase. *Polymer* **2020**, *211*, 123040.
21 Li, C. H.; Jiang, T.; Wang, J. F.; Wu, H.; Guo, S. Y.; Zhang, X.; Li, J.; Shen, J. B.; Chen, R.; Xiong, Y. *In situ* formation of microfibrillar crystalline superstructure: achieving high-performance polylactide. *ACS Appl. Mater. Interfaces* **2017**, *9*, 25818–25829.
22 Sang, Z. H.; Xie, X. L.; Zhou, X. Y.; Li, Y.; Yan, Z.; Xu, L.; Zhong, G. J.; Li, Z. M. Gradient structure of crystalline morphology in injection-molded polylactide parts tuned by oscillation shear flow and its influence on thermo-mechanical performance. *Ind. Eng. Chem. Res.* **2017**, *56*, 6295–6306.
23 Yi, L. F.; Xu, Y.; Li, D.; Shen, J. B.; Guo, S. Y.; Sue, H. J. Fabrication of scratch resistant polylactide with multilayered shish-kabab structure through layer-multiplying coextrusion. *Ind. Eng. Chem. Res.* **2018**, *57*, 4320–4328.
24 Feng, Y. H.; Yuan, Z. X.; Sun, H.; He, H. Z.; Zhang, G. Z. Toughening and reinforcing wood flour/polypropylene composites with high molecular weight polyethylene under elongation flow. *Compos. Sci. Technol.* **2020**, *200*, 108395.
25 He, Y.; Yang, Z. T.; Qu, J. P. Super-toughened poly(lactic acid)/thermoplastic poly(ether)urethane nanofiber composites with *in-situ* formation of aligned nanofibers prepared by an innovative eccentric rotor extruder. *Compos. Sci. Technol.* **2019**, *169*, 135–141.
26 Liu, T.; Lian, X. H.; Li, L. W.; Peng, X. F.; Kuang, T. R. Facile fabrication of fully biodegradable and biorenewable poly(lactic acid)/poly (butylene adipate-*co*-terephthalate) *in-situ* nano-fibrillar composites with high strength, good toughness and excellent heat resistance. *Polym. Degrad. Stabil.* **2020**, *171*, 109044.
27 Chen, Y.; Sun, Z. B.; Li, Y. S.; Lin, H.; Li, Y.; Pan, M. W.; Zhong, G. J.; Li, Z. M. Tuning wettability and mechanical property of polylactide composite films with *in-situ* nanofibrils of poly(butylene adipate-*co*-terephthalate). *Compos. Commun.* **2020**, *22*, 100515.
28 Huang, A.; Peng, X. F.; Turng, L. S. *In-situ* fibrillated polytetrafluoroethylene (PTFE) in thermoplastic polyurethane

(TPU) *via* melt blending: effect on rheological behavior, mechanical properties, and microcellular foamability. *Polymer* **2018**, *134*, 263–274.
29 Lian, X. H. Preparation and properties of *in situ* nanofibrillated PLA blends, Master, South China University of Technology, Guangzhou, **2020**.
30 Chen, Y.; Gao, X. R.; Huang, H. D.; Xu, L.; Ji, X.; Zhong, G. J.; Lin, H.; Li, Z. M. Superhydrophobic, self-cleaning, and robust properties of oriented polylactide imparted by surface structuring. *ACS Sustain. Chem. Eng.* **2021**, *9*, 6296–6304.
31 Zhou, S. Y.; Huang, H. D.; Ji, X.; Yan, D. X.; Zhong, G. J.; Hsiao, B. S.; Li, Z. M. Super-robust polylactide barrier films by building densely oriented lamellae incorporated with ductile *in-situ* nanofibrils of poly(butylene adipate-*co*-terephthalate). *ACS Appl. Mater. Interfaces* **2016**, *8*, 8096–8109.
32 Feng, L. D.; Bian, X. C.; Li, G.; Chen, X. S. Thermal properties and structural evolution of poly(l-lactide)/poly(d-lactide) blends. *Macromolecules* **2021**, *54*, 10163–10176.
33 Gao, X. R.; Li, Y.; Huang, H. D.; Xu, J. Z.; Xu, L.; Ji, X.; Zhong, G. J.; Li, Z. M. Extensional stress-induced orientation and crystallization can regulate the balance of toughness and stiffness of polylactide films: interplay of oriented amorphous chains and crystallites. *Macromolecules* **2019**, *52*, 5278–5288.
34 Zhou, L.; Xu, P. P.; Ni, S. H.; Xu, L.; Zhong, G. J.; Huang, H. D.; Li, Z. M. Superior ductile and high-barrier poly(lactic acid) films by constructing oriented nanocrystals as efficient reinforcement of chain entanglement network and promising barrier wall. *Chinese J. Polym. Sci.* **2022**, *40*, 1201–1212.
35 Xie, Q.; Bao, J. N.; Shan, G. R.; Bao, Y. Z.; Pan, P. J. Fractional crystallization kinetics and formation of metastable *β*-form homocrystals in poly(L-lactic acid)/poly(D-lactic acid) racemic blends induced by precedingly formed stereocomplexes. *Macromolecules* **2019**, *52*, 4655–4665.
36 Xiang, W. K.; Xie, Q.; Xu, S. S.; Sun, C. X.; Yu, C. T.; Zheng, Y.; Pan, P. J. Fractionated crystallization kinetics and polymorphic homocrystalline structure of poly(L-lactic acid)/poly(D-lactic acid) blends: effect of blend ratio. *Chinese J. Polym. Sci.* **2022**, *40*, 567–575.

https://doi.org/10.1007/s10118-022-2880-4